SHAPE PRIOR SEGMENTATION OF MEDICAL IMAGES USING PARTICLE SWARM OPTIMIZATION

Ahmed Afifi, Toshiya Nakaguchi and Norimichi Tsumura
Graduate School of Advanced Integration Science, Chiba University
1-33, Yayoi-cho, Inage-ku, Chiba-shi, Chiba, 263-8522, Japan

Keywords: Liver segmentation, Shape prior segmentation, Optimization for segmentation.

Abstract: The image segmentation is the first and essential process in many medical applications. This process is traditionally performed by radiologists or medical specialists to manually trace the objects on each image. In almost all of these applications, the medical specialists have to access a large number of images which is a tedious and a time consuming process. On the other hand, the automatic segmentation is still challenging because of low image contrast and ill-defined boundaries. In this work, we propose a fully automated medical image segmentation framework. In this framework, the segmentation process is constrained by two prior models; a shape prior model and a texture prior model. The shape prior model is constructed from a set of manually segmented images using the principle component analysis (PCA) while the wavelet packet decomposition is utilized to extract the texture features. The fisher linear discriminate algorithm is employed to build the texture prior model from the set of texture features and to perform a preliminary segmentation. Furthermore, the particle swarm optimization algorithm (PSO) is used to refine the preliminary segmentation according to the shape prior model. In this work, we tested the proposed technique for the segmentation of the liver from abdominal CT scans and the obtained results show the efficiency of the proposed technique to accurately delineate the desired objects.

1 INTRODUCTION

The automatic segmentation of medical images is very essential in almost all medical sites. And consequently several methods have been developed for this purpose (Bankman, 2000), (Dzung, Chenyang, and Jerry, 2000). The traditional methods utilize the intensity changes in order to extract the edges and the local features of the desired objects (Chi and Wang, 2000) or they start with a seed point inside the region of interest and then grow the region by using the similarity measures (Pan and Lu, 2007), (Pohel and Toennies,2001). Despite these methods are helpful in some situations, they are in adequate for medical applications due to the existence of noise, clutter, occlusion and the similarity between objects intensity.

More advanced and a state of the art methods model the segmentation problem as an optimization of energy function (Mcinereny and Terzopoulos, 1996). In these methods, a closed curve deforms until the balance is reached between the internal and the external energy. This curve is represented as a set of control points (Kass, Witkin, and Terzopoulos, 1988) or it is embedded as a zero level in a level set function (Osher and Fedkiw, 2003). Although these methods are more accurate than the traditional methods, the reliance on image information only usually leads to inaccurate results. The inclusion of prior information has shown to improve the segmentation results and recently there is an increased interest in the methods relying on prior information.

In this work, we propose an automated medical image segmentation framework incorporating both shape and texture prior. In this framework the desired texture is efficiently modelled using the over-complete wavelet packet decomposition. In addition, a prior shape model is constructed by the statistical analysis of a set of training shapes describing the variation in object shape. The particle swarm optimization algorithm (PSO) is used to accurately segment the image by adapting the prior shape model according to image features.

After this introduction, In Section2, we will briefly introduce the particle swarm optimization algorithm. In Section3, the proposed segmentation framework will be described deeply. The experimental results will be presented in Section4

Afifi A., Nakaguchi T. and Tsumura N. (2010).
SHAPE PRIOR SEGMENTATION OF MEDICAL IMAGES USING PARTICLE SWARM OPTIMIZATION.
In *Proceedings of the 2nd International Conference on Agents and Artificial Intelligence - Artificial Intelligence*, pages 291-297
DOI: 10.5220/0002724402910297

and the paper will be concluded in Section5.

2 PARTICLE SWARM OPTIMIZATION

PSO is a population based stochastic optimization algorithm founded by Kennedy and Eberhart (1995) . In this algorithm they mimic the social behaviour of bird flocks searching for food to produce computational intelligence. There are many similarities between PSO and the other evolutionary computation techniques, but PSO can achieve better results in a faster, cheaper way compared to other methods (Hassan, Cohanim, and Weck, 2005) .

In PSO, a population or swarm of individuals – particles – are spread over the search space of some problems. Each particle represents a complete solution of this problem and it evaluates the objective function at its location. The particle moves in the search space under the influence of its behaviour and the whole swarm behaviour.

Each particle in the swarm is defined by three *d*-dimensional vectors; the current location $\vec{x}_i$, the velocity $\vec{v}_i$ and the best position it reaches $\vec{p}_i$, where d is the dimensionality of the search space. The original PSO algorithm has been received many enhancements from its appearance till now (Poli, Kennedy, and Blackwell, 2007). The PSO with inertia weight (Clerc, 2006) is one from these enhancements which provides better control on the search space and accordingly, we are interested in it during this work. The PSO algorithm with inertia weight will be described in the following algorithm.

1. Initialize the population array of particles with random position and velocities.

Loop

2. For each particle, evaluate the desired optimization objective function.
3. Comparing particle's fitness evaluation with its $pbest_i$, where $pbest_i$ is the fitness evaluation at particle's best location. If current value is better than $pbest_i$, then set $pbest_i$ equal to the current value, and $\vec{p}_i$ equal to the current location $\vec{x}_i$.
4. Identifying the particle in the neighborhood with the best success so far, and assign its index to variable g.
5. Changing the velocity and position of the particle according to the following equations.

$$\vec{v}_i^{t+1} = \omega\vec{v}_i^{t} + \vec{U}(0,\alpha_1)\otimes(\vec{p}_i - \vec{x}_i) + \vec{U}(0,\alpha_2)\otimes(\vec{p}_g - \vec{x}_i), \quad (1)$$

ω is the inertia weight

$$\vec{x}_i^{t+1} = \vec{x}_i^{t} + \vec{v}_i^{t+1} \quad (2)$$

where:

- t refers to the iteration index.
- $\vec{U}(0,\alpha_i)$ represents a vector of random values uniformly distributed in $[0,\alpha_i]$.
- $\otimes$ is a component-wise multiplication
- v_i is kept within the range $[-V_{max}, +V_{max}]$.

6. If a criterion is met (sufficiently good fitness or maximum number of iteration), exit loop and produce the output.

End loop

The researchers have found that the large value of ω allows the particles to perform extensive exploration and the small value of ω increases the chance to get local optima. So they have found that the best performance could be achieved by using a large value of ω (e.g., 0.9) at the beginning and gradually decrease it until reach another small value of ω.

3 THE PROPOSED FRAMEWORK

The proposed segmentation framework consists of two stages; offline training and online segmentation as shown in Figure1 and as we will demonstrate in the following sections.

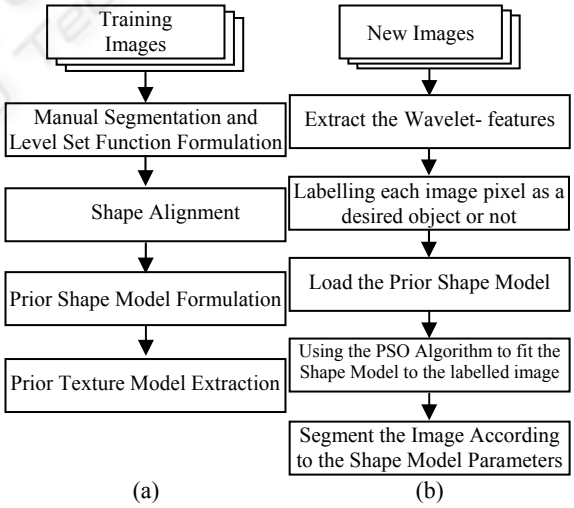

Figure 1: The proposed framework, (a) The offline training stage and (b) The online segmentation stage.

3.1 The Training Stage

3.1.1 Shape Alignment Model

In this work we are interested in aligning binary

images with a value of one inside the object and a value of zero outside. Let we have a training set contains n images $\{I_1, I_2, \dots, I_3\}$, the goal is to calculate the set of pose parameters used to jointly align the binary images. These parameters are defined as a, b, h, θ and they represent the x, y −translation, scaling, rotation respectively. The transformed image of I , based on these pose parameters, is denoted by $\tilde{I}$, and it is defined as

$$\tilde{I}(\tilde{x}, \tilde{y}) = I(x, y), \tag{3}$$

$$(\tilde{x}, \tilde{y}) = \begin{pmatrix} h(x\cos\theta - y\sin\theta) + a, \\ h(x\sin\theta + y\cos\theta) + b \end{pmatrix} \tag{4}$$

An effective strategy to jointly align the binary images is to minimize the following energy functional as defined in [15]:

$$E_{align} = \sum_{i=1}^{n} \sum_{\substack{j=1 \\ j \neq i}}^{n} \left\{ \frac{\iint_{\Omega} \left(\tilde{I}_i - \tilde{I}_j\right)^2 dA}{\iint_{\Omega} \left(\tilde{I}_i + \tilde{I}_j\right)^2 dA} \right\}, \tag{5}$$

where Ω denotes the image domain. Minimizing (5) is equivalent to simultaneously minimizing the difference between any pair of binary images in the training database. The area normalization term in the denominator of (5) is employed to prevent all the images from shrinking to improve the cost function.

Unlike the gradient descent employed in (Tasi et al., 2003), the PSO algorithm can converge to almost global minima. Therefore, in this work we utilize the PSO algorithm to efficiently minimize that energy function as described in the following algorithm.

1. Calculating the mean shape of the training images.
2. Aligning every image to the mean shape using PSO algorithm with a particles constructed from $\{a, b, h, \theta\}$ and (5) as the objective function.
3. Calculating the mean shape of the aligned images and if it is the same as the previous one, end and produce the aligned images; else, go to step2.

To illustrate this alignment process it is applied to a set of 34 binary images of the liver and the overlapping of these images before and after the alignment is shown in Figure2.

3.1.2 Prior Shape Model Formulation

Motivated by the pioneering work of Tasi et al. (2003), we derive the prior shape model from a set of n training images according to the following algorithm.

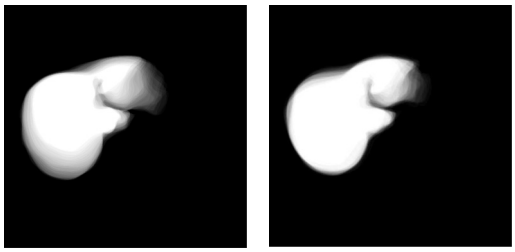

(a) (b)

Figure 2: The amount of shape overlapping in the liver dataset (a) before alignment and (b) after alignment.

1. Deriving the level set functions that describe the desired object from the n training images and denote it as $\Psi_i(x, y)$, $i = 1,2, \dots, n$.
2. Computing the mean level set function $\bar{\Phi}$ from the set of level set functions Ψ_i as

$$\bar{\Phi}(x, y) = {}^1\!/_n \sum_{i=1}^{n} \Psi_i(x, y) \tag{6}$$

3. Deriving the shape variability function according to equation (7).

$$\widetilde{\Psi}_i = \Psi_i(x, y) - \bar{\Phi}(x, y) \tag{7}$$

4. Constructing a column vectors $\psi_i, i = 1,2, \dots, n$ consisting of N samples of each $\widetilde{\Psi}_i$, $N = N_1 \times N_2$ is the image size, by stacking the N_2columns of $\widetilde{\Psi}_i$.
5. Defining the shape variability matrix S as $S = [\psi_1 \quad \psi_2 \quad \dots \quad \psi_n]$.
6. Employing the Eigenvalue decomposition to the shape variability matrix S to compute the variance in shape according to equation (8)

$${}^1\!/_n SS^T = U\Sigma U^T, \tag{8}$$

where U is $N \times n$ matrix whose columns represent the n orthogonal modes of variation in shapes and $\Sigma = diag(\lambda_1, \lambda_2, \dots, \lambda_n)$ is an $n \times n$ diagonal matrix whose diagonals elements represent the corresponding Eigenvalues.

7. Arranging back the N elements of each column of U to yield a maximum of n Eigenshapes or principle modes $\Phi_i, i = 1,2, \dots, n$.

3.1.3 Prior Texture Model Extraction

We utilize the over-complete wavelet packet transform (Wang and Feng, 2005) to extract the high-level feature vectors for each pixel in the training images. The over-complete wavelet packet transform doesn't perform the down-sampling as in

standard wavelet packet transform, so it ensures the translation invariance property which is indispensable for textural analysis. In addition, it provides robust texture features at the expense of redundancy (Li et al, 2005). In this work, we extract the wavelet packet feature set by employing the following algorithm.

1. Applying a two-level over-complete wavelet packet decomposition on the input image.
2. At level-1, select the four sub-bands as feature sub-images.
3. At level-2, in each sub-channel, selecting the sub-band with the maximum variance to be a feature sub-image.
4. Calculating the local energy around each pixel of the feature sub-images as

$$E(x,y) = \frac{1}{(2m+1)^2} \sum_{i=-m}^{m} \sum_{j=-m}^{m} F(x+i, y+j)^2 \qquad (9)$$

where $F(x+i, y+j)$ is the wavelet coefficient of a feature sub-image in the $(2m+1) \times (2m+1)$ window centered at pixel (x, y).

5. Constructing the feature vectors of each pixel in the image from the energy of the corresponding feature sub-images.

After the construction of the high level feature vectors, we assign a label for each pixel to indicate whether this pixel is a desired object pixel or not and finally, we use the linear fisher discriminate algorithm (Franc and Hlavac, 2004) to build the textural prior model.

3.2 The Segmentation Stage

The first step in the segmentation stage is to extract the wavelet packet based feature set of the new image and then classify each pixel in this image as a desired object pixel (true) or undesired object pixel (false) according to the prior textural model. This classification process is carried out by using the linear fisher discriminate algorithm. Finally, this stage is completed by applying the PSO algorithm to get the level set function that truly segments the image as we will clarify in the next sections.

3.2.1 The Model Description

Each particle in the PSO population consists of the set of parameters that control the shape of the segmenting curve. The level set function that implicitly represents the segmenting curve is defined in equation (10).

$$\Phi(x,y) = \bar{\Phi}(x,y) + \sum_{i=1}^{k} w_i \Phi_i(x,y), \qquad (10)$$

where, k is the number of principle Eigenshapes, $w_i, i = 1,2,\dots,k$ are the weights for these Eigenshapes and these weights are ranged from $-\sigma_i \; to \; \sigma_i$ (where σ_i^2 are the Eigenvalues corresponding to these ith Eigenshape). In addition, we consider the pose parameters; a, b for translation, h for scaling, and θ for the rotation angle, which incorporated in this framework using an affine transform. Therefore each particle P in the PSO population is represented as $P = [(w_i, i = 1,2,\dots,k), a, b, h, \theta]$ and it represents a segmenting curve. This segmenting curve can be expressed as the zero level of the level set function defined in equation (13).

$$\Phi(\tilde{x},\tilde{y}) = \bar{\Phi}(\tilde{x},\tilde{y}) + \sum_{i=1}^{k} \Phi_i(\tilde{x},\tilde{y}), \qquad (11)$$

where, $(\tilde{x}, \tilde{y})$ is the new coordinate system obtained using the affine transformation as defined in equation (4).

The fitness of each particle in this work represents how the corresponding curve segments the image. So in the proposed technique, we tend to maximize the fitness function proposed in (Ghosh and Michell, 2006). This fitness function is formulated as:

$$FT = 500(A + (1 - B)), \qquad (12)$$

where, A is the fraction of pixels inside the segmenting curve that are labelled "true" and B is the fraction of the pixels outside the segmenting curve that are labelled "true". The maximization of this objective function means that more desired pixels are gathered inside the segmenting curve.

3.2.2 The PSO Algorithm Configuration

In this work, we are employing the PSO algorithm with inertia weight. The PSO algorithm includes an inertia term and acceleration constants which give us more control on the segmenting curve. The PSO algorithm configuration is shown in Table1 and the curve parameters configuration is practically selected and it can be adjusted according to the desired object. Our parameter configuration is provided in Table2.

Table 1: PSO Algorithm configuration.

Swarm Size (the number of segmenting curves)	25
The Maximum Number of iterations	100
Local Best Influence	2
Global Best Influence	2
Initial Inertia Weight	0.9
Final Inertia Weight	0.4
Number of iterations at which Inertia Weight at Final Value	80

Table 2: Curve Parameters Configuration.

Parameter Name	Parameter Range	Maximum Velocity
$w_i, i = 1,2, \dots, k$	$-\sigma_i \sim \sigma_i$	$\sigma_i/5$
a, b	$-20 \sim 20$	2
h	$0.5 \sim 2$	0.5
θ	$-90 \sim 90$	10

3.2.3 The PSO Algorithm Implementation

After we configure the PSO algorithm and adjust the curve parameters according to the desired object, we carry out the segmentation process according to the following sequence:

1. Initialize the curve parameter randomly from the range specified in Table1.
2. Create the level set function from the curve parameters.
3. Segment the image by all segmenting curves derived from the level set.
4. Measure the fitness of each curve by computing the objective function described in Section 3.2.1.
5. Determine the best segmenting curve and the best segmentation results for each curve.
6. If the best curve is not changed for more than 30 iterations, produce the segmentation results; else go to Step-7.
7. Update the curves parameters according to the PSO algorithm equations and go to Step-2.

4 EXPERIMENTAL RESULTS

In this work we performed two experiments to delineate the liver in abdominal CT scans. In the first experiment, a dataset of five CT images of different patients were used. Each CT image consists of about 150 slices stacked together and the liver fully appears in about 100 slices. In this experiment, 34 key slices were extracted from one patient in the dataset and were manually segmented. The resulting level sets of manually segmented images were used to build the shape prior and textural prior models as described in Section3 and we practically select 8 principle modes to represent the shape variations ($k = 8$). After we had built the shape and textural prior models, we employed the proposed PSO segmentation technique on a set of test slices extracted from the patient used in the training stage as well as a set of test slices extracted from the other patients. Sample results of this experiment are shown in Figure 3 and Figure 4.

In the second experiment, a dataset of ten CT images of different patients were used for cross validation; nine patients were used for training and one patient were used for testing. Each CT image consists of about 170 slices stacked together and the liver fully appears in about 140 slices. In this experiment, key frames were extracted from different patients at interval of 5 slices and all extracted frames were manually segmented. The level sets constructed from corresponding frames were used to build multi shape and texture models. In this work, we use 27 slices to build each model and practically select 7 principle modes to represent the shape variations ($k = 7$). Sample results of this experiment are shown in Figure 5 and Figure 6.

To validate the superiority of the proposed segmentation technique, three competitive techniques were utilized to segment the liver in the same set of slices and all results were compared. The first implemented technique is the active contour without edges (Chan and Vese, 2001) with a manual initialization inside the liver; the second technique performs the segmentation using the wavelet packet decomposition feature set and the fisher linear discriminate algorithm, and the third technique utilizes the genetic algorithm (GA) to fit the pre-constructed shape model as proposed in (Ghosh and Michell, 2006). Figure 7 shows sample results GA-based technique. The goodness of fitness, G, of the segmentation results of all competitive techniques are computed with our experiments and illustrated in Table 3 and Table 4 respectively.

To calculate the goodness of fitness, we generate two binary masks to represent the manual and the computerized segmentation results. These masks have a value of one inside the object and a value of zero outside. Then the goodness of fitness is calculated according to equation (13).

$$G = \frac{|Am \cap Aa|}{|Am \cup Aa|}, \qquad (13)$$

where, Am represents the area of manually segmented object and Aa represents the area of

automatically segmented object. A score of one represents a perfect match with the manual segmentation. As illustrated in Table 3 and Table 4, we note that the proposed PSO segmentation technique gives the best segmentation results.

Table 3: Goodness of fitness, *G*, of the final segmentation results obtained using the different techniques (first experiment).

The segmentation technique	Training patients	Test slices
The proposed technique	0.94	0.88
Active contour without edges	0.70	0.75
Wavelet packet decomposition	0.52	0.45
GA-based technique	0.83	0.78

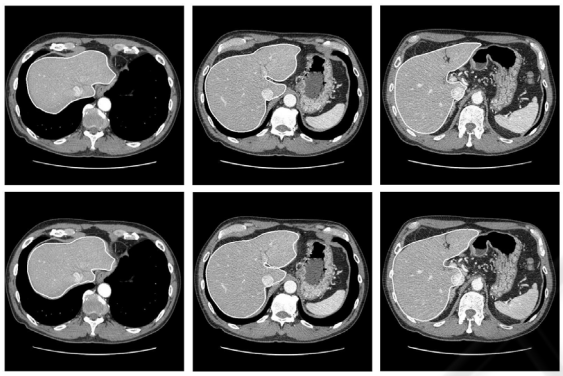

Figure 3: Samples of The proposed technique results, the first experiment, on slices of the same patient used in the training stage, the manual segmentation on the upper row and the results on the bottom row.

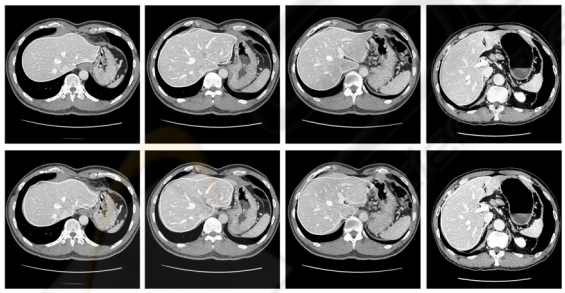

Figure 4: Samples of The proposed technique results, the first experiment, on slices of patients other than the one used in the training stage, the manual segmentation on the upper row and the results on the bottom row.

In addition, the proposed technique did not produce any overlap with the undesired objects and it is not affected by the abnormal tissues as noticed in Figure5 and Figure6.

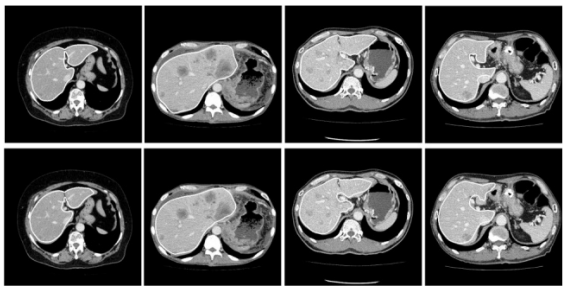

Figure 5: Samples of The proposed technique results, the second experiment, on test slices extracted from the patients used in the training stage, the manual segmentation on the upper row and the results on the bottom row.

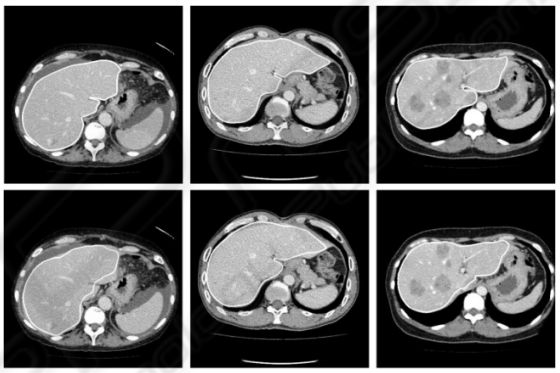

Figure 6: Samples of The proposed technique results, the second experiment, on novel test slices extracted from the test patients, the manual segmentation on the upper row and the results on the bottom row.

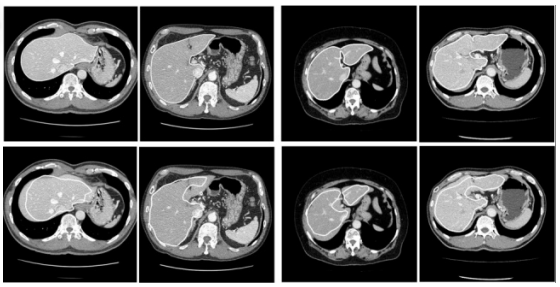

Figure 7: Samples of genetic algorithm-based segmentation technique results, (a) the first experiment, (b) the second experiment, the manual segmentation on the upper row and the results on the bottom row.

Table 4: Goodness of fitness, *G*, of the final segmentation results obtained using the different techniques (second experiment).

The segmentation technique	Training patients	test slices
The proposed technique	0.94	0.92
Active contour without edges	0.72	0.74
Wavelet packet decomposition	0.50	0.48
GA-based technique	0.85	0.79

5 CONCLUSIONS AND FUTURE WORK

In this work, the high level features extracted using the over-complete wavelet decomposition allows the technique to accurately discriminate the desired tissue. Also, the incorporation of prior shape model in the form of mean shape and shape variability as described in Section2 increases the ability to capture the desired object variations without overlapping with the other objects.

Furthermore, the direct optimization using the particle swarm optimization algorithm eliminates the necessitate of deriving gradient of energy or solving complicated differential equations and it does not need level set re-initialization. Moreover, the PSO algorithm can efficiently explore the search space to converge to the desired object and its parameters can be easily adapted for any object. So the proposed PSO segmentation technique is very suitable for the segmentation of abdominal CT scans and it shows promised results. Additionally, the comparison with other techniques shows the superiority of the proposed technique.

REFERENCES

Bankman I. (2000), *hand book of medical imaging, processing and analysis*, academic press.

Chan T., Vese L. (2001), *Active Contour Without edges*, IEEE transactions on image processing, 10(2), 266-277.

Chi Z., and Wang P. (2000), *A New Method of Color Image Segmentation Based on Intensity and Hue Clustering,* 15th International Conference on Pattern Recognition (ICPR'00), 3, 3617.

Clerc M. (2006), *Particle Swarm Optimization*, ISTE Ltd.

Dzung L., Chenyang X., and Jerry L. (2000), *Current Methods in Medical Image segmentation*, Annual Review of Biomedical Engineering, 2(1), 315-337.

Franc V., and Hlavac V. (2004), *Statistical Pattern Recognition Toolbox for Matlab*, Prague, Czech: Center for Machine Perception, Czech Technical University.

Ghosh P., and Michell M. (2006), *Segmentation of Medical Images Using Genetic Algorithm*, Proceedings of the 8th annual conference on Genetic and evolutionary computation, 1171-1178.

Hassan R., Cohanim B., Weck O. (2005) , *A comparison of particle swarm optimization and the genetic algorithm*, 46th AIAA/ASME/ASCE/AHS/ASC Structures, Structural Dynamics, and Materials Conference,1-13.

Kass M., Witkin A., and Terzopoulos D. (1988), *Snakes: Active Contour Models*, International Journal of computer vision, 1(4), 321-331.

Kennedy J., and Eberhart R. (1995), *Particle Swarm Optimization*, Proceedings of the IEEE international conferences on neural networks IV, 1942-1948.

Li Y., Zhang Y., Jiang X., and et al. (2005), *Segmentation of Images Using Wavelet Packet Based Feature Set and Clustering Algorithm*, International Journal of Information Technology", 11(7), 112-121.

McInerney T., and Terzopoulos D. (1996), *Deformable models in medical image analysis: a survey*, Medical image analysis, 1(2), 91-108.

Osher S., and Fedkiw R. (2003), *Level Set Methods and Dynamic Implicit Surfaces*, Springer-Verlag, New York.

Pan Z., and Lu J. (2007), A Bayes-Based Region-Growing Algorithm for Medical Image Segmentation, Computing in Science and Engineering, 9(4)32-38.

Pohle R., and Toennies K. (2001), Segmentation *of medical images is using adaptive region growing*, SPIE Medical Imaging, 4322, 1337–1346.

Poli R., Kennedy J, and Blackwell T. (2007), *Particle Swarm Optimization: An Overview*, Springer Journal of Swarm Intelligence, 1, 33-57.

Tasi A., Yezzi A., Wells W., and et al. (2003), "*A Shape-Based Approach to the Segmentation of Medical Imagery Using Level Sets*, IEEE transaction on medical imaging, 22(2), 137-154.

Wang Q., and Feng D. (2005), *A Novel Texture Descriptor Using Over-Complete Wavelet Transform and Its Fractal Signature*, Lecture Notes in Computer Science, 3568, 476-486.